Upwelling filaments off Cap Blanc: Interaction of the NW African upwelling current and the Cape Verde frontal zone eddy field?

T. Meunier,[1] E. D. Barton,[2] B. Barreiro,[2] and R. Torres[3]

Received 20 January 2012; revised 31 May 2012; accepted 29 June 2012; published 25 August 2012.

[1] The hydrographical and dynamical properties of the upwelling filaments forming off Cap Blanc (Mauritania) are investigated using remotely sensed and in situ data collected in April/May 2009 during the strongest upwelling season. The area is situated at the southern edge of the NW African upwelling system, where the Cape Verde Frontal Zone (CVFZ) separates warmer, saltier North Atlantic Central Water (NACW) and cooler, fresher South Atlantic Central Water (SACW). Sea surface temperature images indicated the presence of an upwelling filament extending >280 km offshore, rooted over the Cap Blanc promontory and entrained around a warm-core anticyclonic eddy. After this filament started to decay, a new cold filament developed at the approximate same location. High resolution Moving Vessel Profiler (MVP) and Acoustic Doppler Current Profiler (ADCP) surveys of these mesoscale structures revealed that both filaments were carrying South Atlantic Central Water (SACW) offshore through an intense jet-like flow. Similarity of the relative vorticity structure across the filament with that of the tangent eddy suggested that the latter was responsible for the offshore current. Tracking of this eddy in altimetric data demonstrated that it originated from the CVFZ, as implied by its hydrographic structure. Altimetric data also revealed that another anticyclonic structure centered over the Cap Blanc promontory was responsible for the northwestward advection of SACW into the base of the filament. The results support the idea that some upwelling filaments can be produced by the interaction of an external eddy field, including topographic eddies, with the upwelled water.

Citation: Meunier, T., E. D. Barton, B. Barreiro, and R. Torres (2012), Upwelling filaments off Cap Blanc: Interaction of the NW African upwelling current and the Cape Verde frontal zone eddy field?, *J. Geophys. Res.*, *117*, C08031, doi:10.1029/2012JC007905.

1. Introduction

1.1. Upwelling Filaments

[2] Eastern boundary upwelling systems are zones of intense baroclinic alongshore currents associated with sharp coastal density fronts. Early satellite imagery revealed the existence of mesoscale cross-shore structures along the upwelling front [*Traganza et al.*, 1980]. These tongues of cold upwelled water, extending hundreds of kilometers offshore became known as upwelling filaments [*Brink*, 1983; *Flament et al.*, 1985]. They were intensively studied from the eighties using in situ and remotely sensed data, mainly in the California current system [*Brink*, 1983; *Flament et al.*, 1985; *Washburn and Armi*, 1988; *Dewey et al.*, 1991; *Strub et al.*, 1991; *Ramp et al.*, 1991]. They have been since observed in every major upwelling system: Benguela [*Shillington*, 1990; *Lutjeharms et al.*, 1991], Iberia [*Haynes et al.*, 1993; *Relvas and Barton*, 2002; *Barton et al.*, 2001; *Peliz et al.*, 2002], Humboldt [*Marin et al.*, 2001; *Sobarzo and Figueroa*, 2001], and north-west Africa [*Gabric et al.*, 1993; *Navarro-Perez and Barton*, 1998; *Kostianoy and Zatsepin*, 1996; *Barton et al.*, 2004; *Knoll et al.*, 2002] and have been shown to be an important source of offshore transport [*Kostianoy and Zatsepin*, 1996] from the nutrient-rich coastal water to the oligotrophic open ocean [*Alvarez-Salgado et al.*, 2001]. One of their particularities is their tendency to form recurrently at some particular locations along the coast, often near large capes, but sometimes also along straight coast lines [*Haynes et al.*, 1993; *Kostianoy and Zatsepin*, 1996].

[3] Many numerical studies have focused on the dynamics of upwelling filaments, highlighting the variety of physical processes possibly responsible for their formation and evolution. The formation of steep meanders through intrinsic baroclinic instability of the upwelling front was investigated by *Ikeda and Apel* [1981], *Ikeda et al.* [1989], *Haidvogel et al.* [1991], *Batteen* [1997], *Capet et al.* [2002], *Marchesiello et al.* [2003], *Capet and Carton* [2004], *Batteen et al.* [2007], and *Meunier et al.* [2012]. They all agreed in the meander-like

[1]Laboratoire de Physique de l'Océan, Ifremer, Plouzané, France.
[2]Instituto de Investigaciones Marinas de Vigo, Vigo, Spain.
[3]Plymouth Marine Laboratory, Plymouth, UK.

Corresponding author: T. Meunier, Laboratoire de Physique de l'Océan, Ifremer, Pointe du Diable, FR-29280 Plouzané, France. (thomasmeunier@iim.csic.es)

0148-0227/12/2012JC007905

nature of the filaments, but some studies differed on the role of the coast-line geometry and the bottom topography especially in the trapping of the filaments. While *Haidvogel et al.* [1991] suggested that irregularities in the topography were necessary to trigger the instability, *Marchesiello et al.* [2003] noted that eddies and filaments could develop over a flat bottom and a straight coast line, in agreement with *Røed and Shi* [1999]. They only noted an anchoring of the filamentary structures near capes, similar to the conclusions of *Batteen* [1997] and *Batteen et al.* [2007]. Noting that unstable meanders of buoyancy driven coastal currents propagated downstream [*Ikeda and Apel*, 1981; *Ikeda et al.*, 1989], *Meunier et al.* [2010] investigated the mechanism responsible for the repeated occurrence and the trapping observed at some particular locations, even in the case of a straight coast line. They found that bottom topographic features like promontories were able to generate potential vorticity anomalies (PVA) in the form of trapped anticyclones. When interacting with the upwelling front, these topographic eddies formed long trapped filaments. The interaction between deep eddies and a surface boundary current was also shown to produce coastal water filaments in the Iberian upwelling system: *Peliz et al.* [2004] observed that meddies (anticyclones of Mediterranean water) and dipoles of Mediterranean water were able to generate extremely long filaments of coastal origin off Cape Sao Vicente even in the absence of upwelling. *Serra et al.* [2010] used remotely sensed data and a realistic numerical model to demonstrate that these meddies could interact with the upwelling front and generate upwelling filaments further north along the western Iberian coast. The interaction of these deep structures and the surface current were investigated in a simple model framework by *Meunier et al.* [2012], who showed that deep eddies could interact with the surface flow even when they are separated with a mid-depth zero-Potential Vorticity Anomaly layer.

[4] *Strub et al.* [1991] differentiated upwelling filaments into three categories, according to their dynamical cause : squirts, which are small filaments possibly generated by coastal convergence [*Stern*, 1986]; unstable meanders, as discussed above; and the interaction of the upwelled front with an external mesoscale eddy field. They insisted on the non-mutually exclusive nature of these processes. In every case, filaments result from the interaction between a vortical structure, (near surface or at deeper levels, whether intrinsic to the current or from an external source) and a coastal front.

1.2. The Cap Blanc Region

[5] Cap Blanc (Mauritania) is situated at about 21°N 17°W, just north of the Banc d'Arguin, in the southern part of the north-west African upwelling system (Figure 1a), where upwelling-favorable winds are strong all year long though intensified in spring. The NW African current system exhibits all the typical features of an upwelling system : a baroclinic near surface jet associated with the upwelling front [*Barton et al.*, 1977], accompanied by mesoscale activity in the form of meanders and eddies [*Barton*, 1987, 1998; *Barton et al.*, 2004; *Kostianoy and Zatsepin*, 1996], and a poleward countercurrent along the slope between 200 and 300 m [*Hughes and Barton*, 1974; *Barton et al.*, 1982; *Mittelstaedt*, 1991]. A particularity of the southern NW African upwelling system is the weak stratification of the water column, resulting from the presence of decreasing salinity below the pycnocline. This weak stratification results in less available potential energy, and therefore less energy conversion into eddy kinetic energy through baroclinic instability than other upwelling systems like the California Current System [*Marchesiello and Estrade*, 2009].

[6] The Cap Blanc area is also situated within the boundary zone between the relatively salty North Atlantic Central Water and the fresher South Atlantic Central Water [*Mittelstaedt*, 1991]. The NACW and SACW form a well defined zonal front all across the tropical North Atlantic, which takes a south-west/north-east orientation from the Cape Verde islands longitude to the African coast [*Sverdrup et al.*, 1942; *Fraga*, 1974; *Emery and Meincke*, 1986]. This strong salinity front off NW Africa (Figure 1c) was named by *Zenk et al.* [1991] as the Cape Verde Frontal Zone (CVFZ). The frontal zone was defined in vertical coordinates as the intersection of the 36 psu isohaline and the 150 m level [*Barton*, 1987; *Zenk et al.*, 1991], and is also clear in isopycnic coordinates as a strong salinity gradient along the 26.5 to 26.8 isopycnal surfaces [*Perez-Rodriguez et al.*, 2001]. The compensation of the salinity and temperature contributions in the density results in a weak density front. Despite the weak currents expected from the weaker density gradients, mesoscale variability was observed in the frontal region in the form of interleavings of water masses [*Perez-Rodriguez et al.*, 2001; *Martínez-Marrero et al.*, 2008]. A numerical study from *Onken and Klein* [1991] showed that the presence of mesoscale patterns in the frontal zone was related to baroclinic instability, with a wavelength of 200 km for the fastest growing mode. The destabilization of the front results in the formation of mesoscale eddies. The variability associated with this destabilization has spatial scales of the order of 100 km. At mid-depth, below 1000 m, Rossby waves dominate the variability and topographic Rossby waves associated with the Cape Verde plateau are likely to be found in the bottom layers [*Spall*, 1992]. *Erasmi et al.* [1998] examined the energy terms and energy transfer terms from numerical model results and mooring data and confirmed that eddy kinetic energy (EKE) dominated the kinetic energy (KE) in the frontal zone, and that the transfer from potential energy (PE) to EKE, consistent with baroclinic instability, was important. An underestimation of the EKE by the model compared to the in situ data, along with an important increase of the EKE when increasing the resolution of the model suggested that sub-mesoscale structures are an important source of EKE in the region, similar to the results obtained by *Capet et al.* [2008a, 2008b, 2008c] in the California region. Strong isopycnal and diapycnal mixing were observed in the frontal zone, probably associated respectively with a downward energy cascade from mesoscale to small scale and vertical shear instability processes [*Tomczak*, 1981; *Klein and Siedler*, 1995]; *Martínez-Marrero et al.*, 2008].

[7] The intersection of the Mauritanian coastal upwelling system and this frontal area is a complex and dynamic zone, as intrinsically unstable currents associated with upwelling interact with the Cape Verde front eddies. The hydrography also becomes complicated, as both SACW and NACW may be upwelled and mixed laterally.

1.3. Aim and Scope of the Present Paper

[8] In this paper, the nature and dynamics of the large filaments forming off Cap Blanc are investigated using in situ

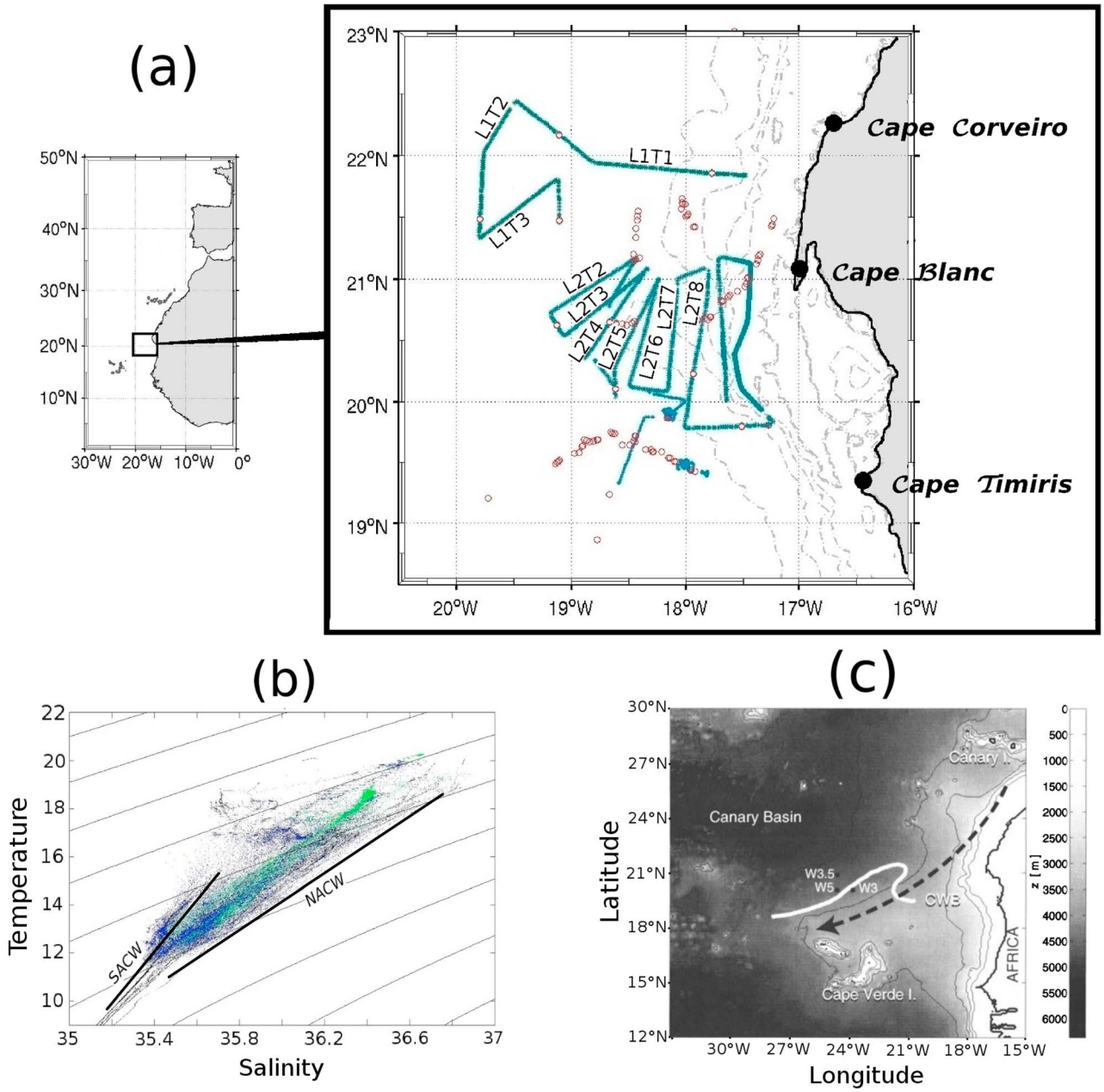

Figure 1. (a) Cruise map: MVP transects are plotted as colored thick lines, labeled for reference. Red circles represent CTD stations. (b) TS-diagram of all CTD and MVP casts during the cruise. (c) Schematic map of the Cape Verde front position (continuous white line) from *Erasmi et al.* [1998].

data collected in the frame of the interdisciplinary SOLAS-ICON project on Discovery Cruise 338. Two quasi-synoptic mesoscale surveys were performed with *Moving Vessel Profiler*, CTD, ADCP and drifters to sample the structure of the upwelling filaments and surroundings, in support of several Lagrangian, tracer and gas exchange experiments. The present aim is to establish an Eulerian view of their temperature, salinity, density and spiciness fields as well as their relationship with the current velocity field.

[9] In section 2, we present the sampling strategy, data, instruments used and processing steps. The results are presented in section 3 where remotely sensed Sea Surface Temperature images (section 3.1) are used to put in context the in situ data. The latter are then presented in two subsections. The first documents the hydrographical and dynamical structure of a large anticyclonic eddy with an extended filament entrained around it (section 3.2). The second explores a newly formed upwelling filament mapped three-dimensionally on fine scale (section 3.3). The results are discussed in section 4 and conclusions are drawn.

2. Data

2.1. In Situ Data

[10] Two surveys with continuous Moving Vessel Profiler (MVP) and Acoustic Doppler Current Profiler (ADCP)

observations mapped the three dimensional hydrographic structures of the large upwelling filaments developing off the Cap Blanc shelf and the associated currents (Figure 1a). The surveys alternated with Lagrangian experiments in which drifters released in the filaments were followed by the ship and CTD stations were performed along their tracks. The first survey took place from 14 to 20 April 2009. An MVP problem during this survey allowed only two full hydrographic sections across the long filament, but the survey was completed collecting ADCP data. The second survey was performed using MVP and ADCP from 30 April to 5 May along nine full cross-filament transects.

[11] The MVP is composed of a CTD-equipped fish, which dives almost vertically down to 350 m, with the aid of a powerful computer-controlled winch as the ship moves at a speed of 7 knots. The winch then hauls the profiler obliquely back to the surface before the next new vertical dive. The horizontal resolution (distance between two drops) was between 1500 and 2000 m depending on the cast depth. This system is faster than conventional CTD stations, and thus improves synopticity of the 3-dimensional mapping. The following instruments were mounted : *Applied Microsystems Laboratory (AML) Oceanographic* micro CTD, *AML Oceanographic* micro dissolved oxygen, *Chelsea instruments* MINITracka fluorimeter, and *Satlantic* irradiance sensors. The MVP sensor suite was calibrated prior to the cruise, during which it was compared with CTD casts at the start and end of deployments and with the near surface underway sensors each time it approached surface. In general, instrument performance was within manufacturers' specifications, but during the second survey, a step change in salinity occurred on the fourth transect. Comparison with the underway data and subsequent CTD casts indicated a constant offset, which was corrected. The MVP data were then interpolated onto regular grids using the Barnes algorithm [*Barnes*, 1994] for plotting purposes.

[12] Isopycnic coordinates, which use the density referred to surface pressure ($\sigma_0 = \rho(S, T, P = 0) - 1000$) as a vertical coordinate, are largely used in this paper. They are a natural coordinate system to use in the ocean because most dynamically relevant parameters are conserved along an isopycnal path. They are also convenient as they filter out most internal gravity waves. Because the data are here described in isopycnic coordinates, the 'horizontal gradients' discussed below are derivatives along a chosen isopycnal surface and not strictly horizontal. The density was calculated using the UNESCO algorithms [*Fofonoff and Millard*, 1983].

[13] The spiciness variable [*Flament*, 2002] is used in the description of the hydrographic situation. It is the orthogonal function of density anomaly in the T,S space. High spiciness water thus corresponds to warm and salty water whereas low spiciness water corresponds to fresh and cool water. This variable is of prime interest in the case of two water masses with density compensating contribution of their respective temperature and salinity, where the spiciness remains a good tracer of the water masses.

[14] Current data were obtained along the ship track during the whole cruise with two shipboard Acoustic Doppler Current Profilers (ADCP). One was an RDI 150 KHz Broadband ADCP and the other an RDI 75 KHz Broadband ADCP, both with transducers mounted 5 m below the water line. The ping rate was 1 Hz for both instruments and the maximum sampled depth was 750 m from the 75 KHz system and 330 m from the 150 KHz system. The data acquisition system consisted of two Pentium 4-PC compatible computer running the RDI VMDAS program. This program integrated the satellite GPS navigation into the ADCP system. ADCP processing used the Common Oceanographic Data Access System (CODAS), developed at the University of Hawaii [*Firing et al.*, 1995]. In general, the ADCP data were of good quality with only occasional data loss due to intermittency in the navigation input to VMDAS.

[15] The Pacific Gyre surface drifters used here comply to the standard WOCE configuration of a cylindrical surface buoy equipped with ARGOS and GPS radio transmission and drogued with a standard Holey Sock of 6 m length and 1.5 m diameter. The drogues were nominally centered at 12 m from the surface. The drifters' positions were followed both from the GPS radio signal and from the ARGOS positioning system.

2.2. Remotely Sensed Data

[16] Daily (except for a few cloudy days) sea surface temperature (SST) maps of the Cap Blanc area were provided by the PML remote sensing group. The processing of the images, derived from 1 km resolution AVHRR data, is detailed at http://rsg.pml.ac.uk/.

[17] Maps of absolute dynamic topography were obtained from IFREMER-CERSAT. They are distributed by the AVISO Web site (http://www.aviso.oceanobs.com/en/altimetry/index.html), where details of processing may be found. The spatial resolution is of 25 km.

[18] Remotely sensed wind data (Quickscat) were produced by the NASA Physical Oceanography Distributed Active Archive Center, at Jet Propulsion Laboratory, California Institute of California (JPL/PO.DAAC). They were distributed by the CERSAT service as a mirror site for Europe. (http://cersat.ifremer.fr/Data/Discovery/By-product-type/Swath-products/QuikSCAT-L2B).

3. Results

3.1. Context and Remotely Sensed Data

[19] The wind off Cap Blanc was steady and upwelling favorable (equatorward) most of the year, as shown in Figures 2a and 2b, but particularly intense in spring. The wind measured by both ship and QuikScat was upwelling favorable during the whole cruise even though its intensity occasionally decreased during short periods (Figures 2c and 2d).

[20] Figure 3 shows the SST evolution on 12, 15, 18, 21, 27 April, 1 and 3 May. On 12 April, a long cool (18°C) filament (labeled A) with a convoluted meandering base between 20.5 and 21.2°N, near 18°W, was linked to a cold meander of the upwelling front above the Cap Blanc promontory. Filament A extended 280 km offshore from the coast as a thin tongue of cool water. North of this long filament, a shorter, sharp meander of the upwelling front centered at 22.3°N 17.8°W formed filament B. After a significant growth from 12 to 15 April, filament B evolved into a mushroom-like (or hammer head) structure on 18 April, under the influence of a large warm-core anticyclonic eddy centered at 22°N 19°W. Simultaneously, the tip of filament A was entrained around the anticyclone while its base meandered increasingly,

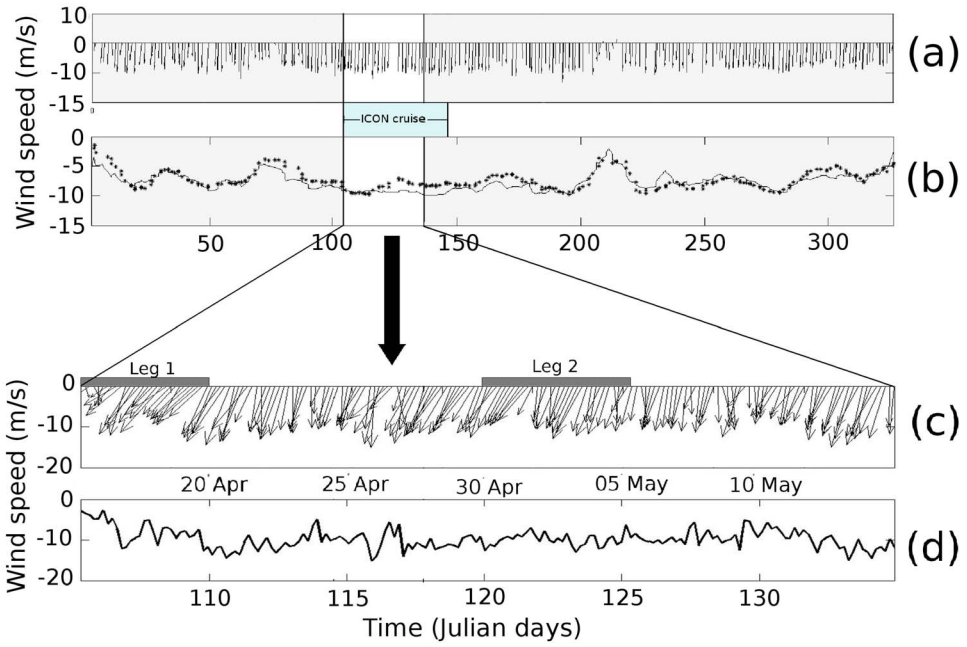

Figure 2. (a) Wind vectors for 2009 at 21°N 18°W from the Global Forecasting System atmospheric model. (b) Northward component of modeled wind (solid line) and QuikScat observations at the same point. (c) Wind vectors and (d) northward component of wind observed on board Discovery between 14 April and 15 May 2009.

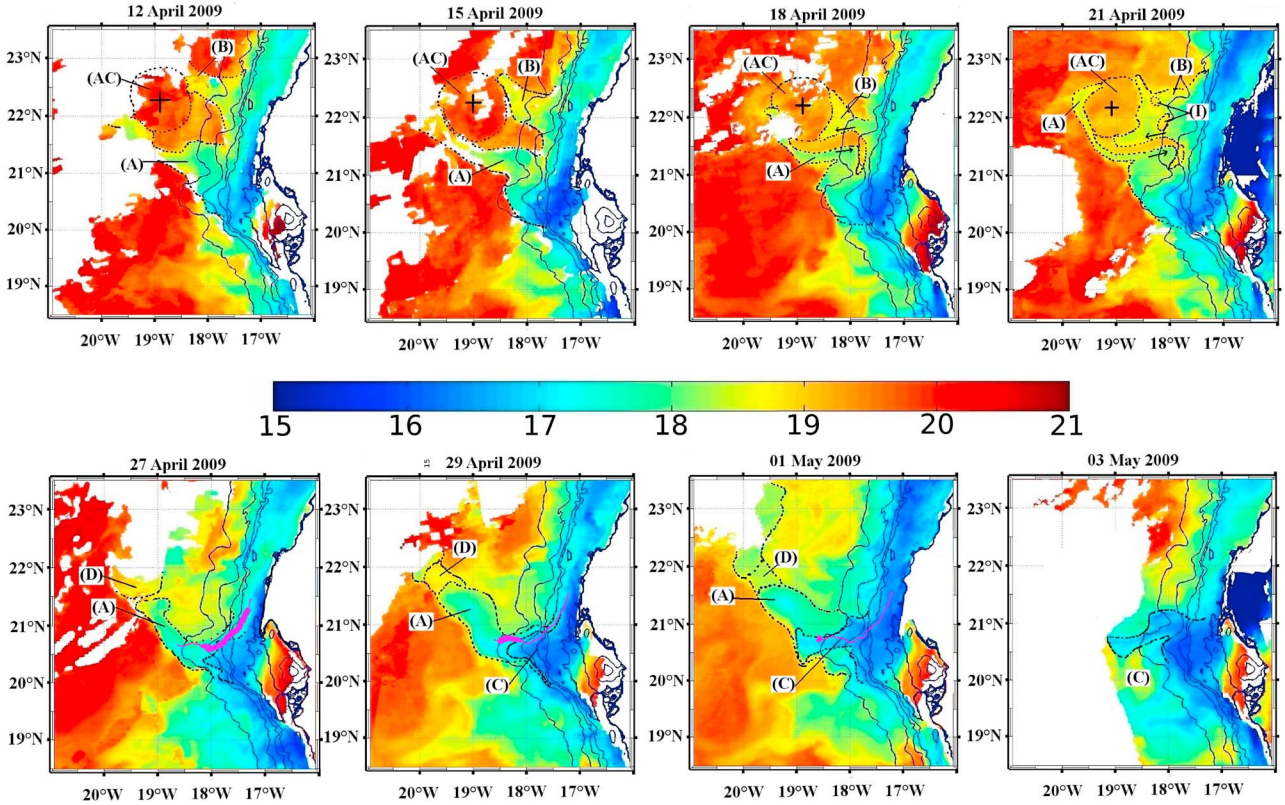

Figure 3. AVHRR Sea Surface Temperature maps from mid-April to early May. The eddy and filament are contoured with a dotted line. Labeled structures are filament A (labeled A), filament B (labeled B), the anticyclone (labeled AC), whose center is marked with a cross; filament C (labeled C), detachment of filament A's tip (labeled D), and the intrusion of warmer water within filament B (labeled I). Drifter trajectory is superimposed on the 27 and 29 April and 01 May maps as a magenta line (thicker for the current day).

anticyclonically over the Cap Blanc promontory and cyclonically near 21.3°N 18°W .

[21] A complex situation arose on 21 April, when the contorted base of filament A became separated from filament B by only a narrow strip of warm water. At the same time, the offshore tip of filament A continued to extend offshore to reach 22.5°N 19.7°W. The anticyclone was almost entirely surrounded by cool upwelled water as filament B broadened during the same time. Two small patches (10 km) of warmer water became caught within filament B as the latter broadened into a large hammer-head shape.

[22] Three drifters were released on 22 April at 21.48°N 17.25°W, near the upwelling front. All three drifters followed similar trajectories and therefore, only one will be discussed. As no cloud-free images were available from 22 to 26 April, the trajectory is shown superimposed on the SST images of 27 and 29 April and 1 May. The thin magenta line represents the entire trajectory from 22 April to 1 May, while the thick line represents the trajectory since the last available SST image. Although drogued in the Ekman layer, all three drifters traced the temperature front, heading south-west because of the cold front curvature over the promontory, with irregular velocities ranging from 0.3 to 0.6 m.s^{-1} from 22 to 27 April. The image of 27 April shows a separation of filament A's extended tip, and of the hammer-head like tip of filament B (Figure 3). Both were discernible as a patch of cool water offshore , but the anticyclone was no longer clearly discernible in the SST images. Following this detachment, probably the consequence of its westward drift, filament A's contorted base evolved into a shorter, slightly curved cool filament, still rooted on the large cold meander over the Cap Blanc promontory. Drifters had at that time reached the offshore boundary of the cold meander above the Cap Blanc promontory. Smaller scale SST structures are discernible on the large, cold meander, confirming the strong sub-mesoscale activity of the region.

[23] SST images from 29 April to 1 May (Figure 3) show an offshore spreading of the recently upwelled cold water from the cold meander into the previous position of filament A. It is unclear whether this new tongue of upwelled water was a renewal of filament A, as both structures seem to emerge from the cold water pool situated at the base of the Cap Blanc promontory. Here it is referred to as filament C.

[24] The drifters moved approximately at the same velocity as the offshore tip of the cold meander as it evolved into the filamentary structure. They were recovered on 1 May. On 1 May, the tip of filament C turned northward almost perpendicularly. The base of the filament meandered increasingly and moved north-westward, consistent with entrainment around a cyclonic eddy, so that on 3 May, the recently formed cold filament was less coherent, with a general north-westward drift and minor filament structures south of the main filament. Two shorter filaments south of the Cap Blanc promontory, developing just west of the Banc d'Arguin from 12 April (Figure 3) are advected or propagate northward until 3 May, and may be partly responsible for the smaller scale meanders observed along filament C.

[25] The SOLAS-ICON experiment illustrates two situations: the entrainment of upwelled water around an anticyclonic eddy (filament A), and the formation of a new upwelling filament over the Cap Blanc promontory (filament C), rooted at the same location.

3.2. Filament A: Entrainment of Upwelled Water Around an Anticyclonic Eddy

3.2.1. The Anticyclone AC

[26] The anticyclonic eddy (AC) and filament A were surveyed using MVP and ADCP. The anticyclone AC is visible in the density section shown in Figure 5c: Near the surface, it is evident as a 100 km wide lens of lighter water ($\sigma_0 < 26.1$) centered at 18.8°W. Below the light water lens the isopycnals are compressed so that the water column is well stratified with a strong pycnocline (between $\sigma_0 = 26.1$ and $\sigma_0 = 26.2$) between 50 and 70 m. Below 120 m, the isopycnals have a general basin like shape from 18.4 to 19.4°W, but an upward doming around 19°W complicated the pattern. The eddy also has a strong signature in terms of spiciness, temperature and salinity which are shown in isopycnic coordinates respectively in Figures 5d–5f. The upper core is associated with warmer (>20°C) and saltier (>36.6 psu) water between the 26.2 isopycnal and the surface. Between the 26.2 and 26.4 isopycnals, interleavings of contrasting salinity and temperature are evident below the warm water lens. At mid depth, between the 26.4 and 26.8 isopycnals, the temperature and salinity distribution is almost homogeneous along the isopycnal surfaces. A dome of fresher, colder water is situated between the 26.8 and 27 isopycnals, between 300 and 350 m, centered at 19°W, coincident with the upward dome of the isopycnals. A TS diagram is shown in Figure 5b. The color of each data point refers to its position along the section, which can be deduced from the reference color bar over Figure 5d. It shows that the water mass found inside the eddy core (light blue to light green points) ranges from SACW in depth to NACW near the surface, whereas the waters found near the shelf break are closer to NACW throughout the water column.

[27] Figure 4 shows the 32 and 288 m current vectors superimposed on a SST map of 15 April. The typical eddy velocity distribution, with a flow reversal in the center of the circled warm water mass is obvious. The vertical distribution of the eddy tangential velocity is shown in Figure 5g. Near the surface, it increases from near-zero at the south-eastern edge of the eddy near 18.4°W, reaches -0.3 m.s^{-1} at 18.7°W, and then quickly reverses at the exact location of the warm core. The velocity increases and reaches 0.42 m.s^{-1} near 19.3°W, and decreases again at the end of the section. Even though the velocity appears to be slightly intensified in the first 70 m, it varies little with depth between 70 and 280 m. A cross section of the relative vorticity is shown in Figure 5h. Noting that the velocity within the eddy is almost fully tangential, (i.e. perpendicular to the radial section), the relative vorticity along the sampled line can be approximated as: $\zeta_r = \partial_r u_\theta + u_\theta/r$. The anticyclonic structure is clearly identifiable between 19.2 and 18.8 °W as a column of strong negative relative vorticity, intensified within the first 100 m, with a maximum value of about 2.5×10^{-5} or half the Coriolis parameter. Below 100 m, the vorticity varies little, ranging between 1.2 and 1.8×10^{-5} s^{-1}. The negative vorticity associated with the core of the eddy is surrounded by two surface-intensified cores of positive relative vorticity.

[28] The good agreement between the eddy's depth-averaged relative vorticity profile and an idealized barotropic Gaussian eddy from *Carton and Legras* [1994] (not shown) suggests that the positive vorticity cores surrounding the

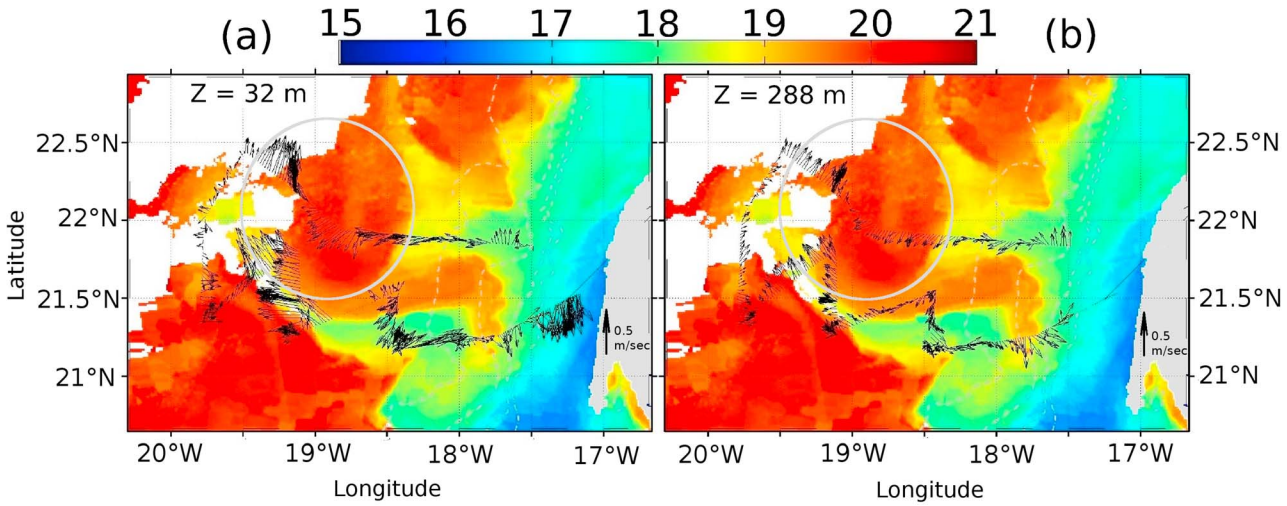

Figure 4. Current vectors at (a) 32 and (b) 288 m superimposed over the SST map on 15 April. White circle highlights the anticyclonic eddy.

anticyclonic eddy are associated with a vorticity crown inherent in typical Gaussian eddies.

[29] The eddy was followed using weekly altimetric data (absolute dynamic topography) from its generation to its drift far offshore (Figure 6). It was seen to be generated from the growth of a perturbation during the unstable interaction between two anticyclones west of Cap Blanc in early February. In March, the perturbation had grown into a small isolated anticyclonic anomaly centered near 23°N 18.5°W. It then continued to strengthen, and became a coherent anticyclonic eddy in April, reaching a diameter of about 100 km by the time of the in-situ sampling. It subsequently drifted westward far from the eastern boundary, and was observable until end of September in the western North Atlantic, attaining a total life cycle of more than 240 days. The fact that this anticyclone arose from the unstable interaction of two previously formed eddies in the vicinity of a well known turbulent front and that both water masses could be found within the eddy strongly suggests that this anticyclone driving the filament formation is directly related with the dynamics of the Cape Verde Frontal Zone.

3.2.2. The Long, Entrained Filament (A)

[30] Filament A was evident in the SST images as a long, narrow, cool feature around 18.5°C entrained around the anticyclone AC. The filament is obvious in the hydrographic section as the outcropping of the 25.9 to 26.1 isopycnals around 19.3°W (Figure 7c). Between 100 and 70 m, the 26.3 and 26.2 isopycnals dome gently, with a general rise from west to east across the section. At all depths sampled below 100 m, all isopycnals dome more strongly, with a mean displacement of about 50 m. The center of this dome (19.45°W) is shifted from the outcropping center. Temperature (Figure 7e) and salinity (Figure 7f) show a clear diapycnal distribution, with both isotherms and isohalines crossing the isopycnal levels from 350 m to the surface. This steep rise of isotherms and isohalines is evident in the temperature and salinity isopycnic sections as a vertical strip of cool, low salinity (and thus low spiciness) water in isopycnic coordinates, extending from 19.40 to 19.55°W. This hydrographic signature of filament A indicates the introduction of a narrow but thick body of water with contrasting properties. It is evident in the TS diagram (Figure 7b) as the lower salinity signature of the light green points corresponding with the filament's position. On both sides of the filament, large masses of saltier and warmer water extend over the 26.45 isopycnals. The warm and salty water to the east of the section, visible in the TS diagram as dark blue points, have hydrographic properties close to those of the anticyclonic eddy water.

[31] The filament was associated with strong westward velocities in a surface-intensified jet-like offshore flow in the central section (L1T3), as seen in Figure 4. This flow persisted throughout the cool anomaly except at its tortuous base where smaller scale processes seem to dominate. A weaker opposed return flow was present south of the filament. The vertical structure across the central section is shown in Figure 7g. The offshore jet reaches a maximum velocity of 0.5 $m.s^{-1}$ in the upper 50 m. Although it is surface intensified, flow remains intense (between 0.25 and 0.4 $m.s^{-1}$) down to 280 m. The horizontal velocity shear related to the jet-like profile and the reversal of the flow south of filament is also stronger near the surface with values reaching 2.5×10^{-5} s^{-1} but remains intense throughout the sampled water column. The velocity being almost fully perpendicular to the section, this horizontal shear is a good approximation for the relative vorticity (Figure 5h). The filament and eddy vorticity signals are indistinguishable, which implies that the filament is essentially an advective feature entrained around the eddy.

3.3. The Recently Formed Filament C

[32] As mentioned in section 3.1, filament C started growing from the base of filament A over the Cap Blanc promontory shortly after a re-intensification of the wind. A high resolution 3D mapping of its hydrographical and dynamical properties was completed between 30 April and 5 May using ADCP and MVP. Absolute dynamic topography and the associated geostrophic velocity field on 06 May are shown in Figure 8. The surveyed area is indicated by the outlined polygon. An anticyclone centered at 21°N just west of Cap Blanc, over the promontory, is obvious in both

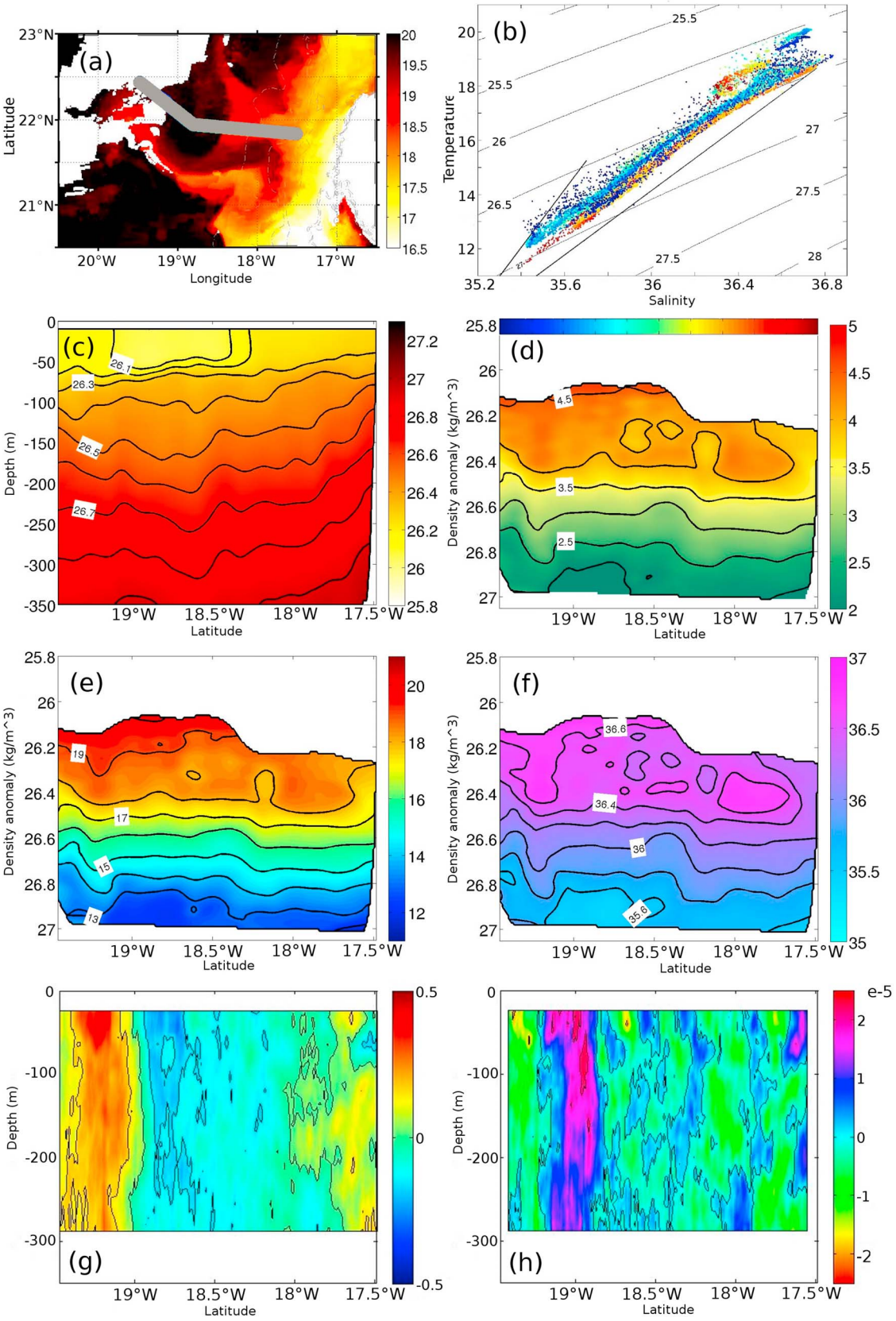

Figure 5. (a) Section L1T1 location superimposed on SST map of 15 April. (b) TS diagram for transect in which data point locations are indicated by the reference colors superimposed on the section trajectory above Figure 5d. Vertical sections of (c) density against depth and (d) spiciness, (e) temperature and (f) salinity against density across the eddy. (g) Current speed and (h) relative vorticity against depth.

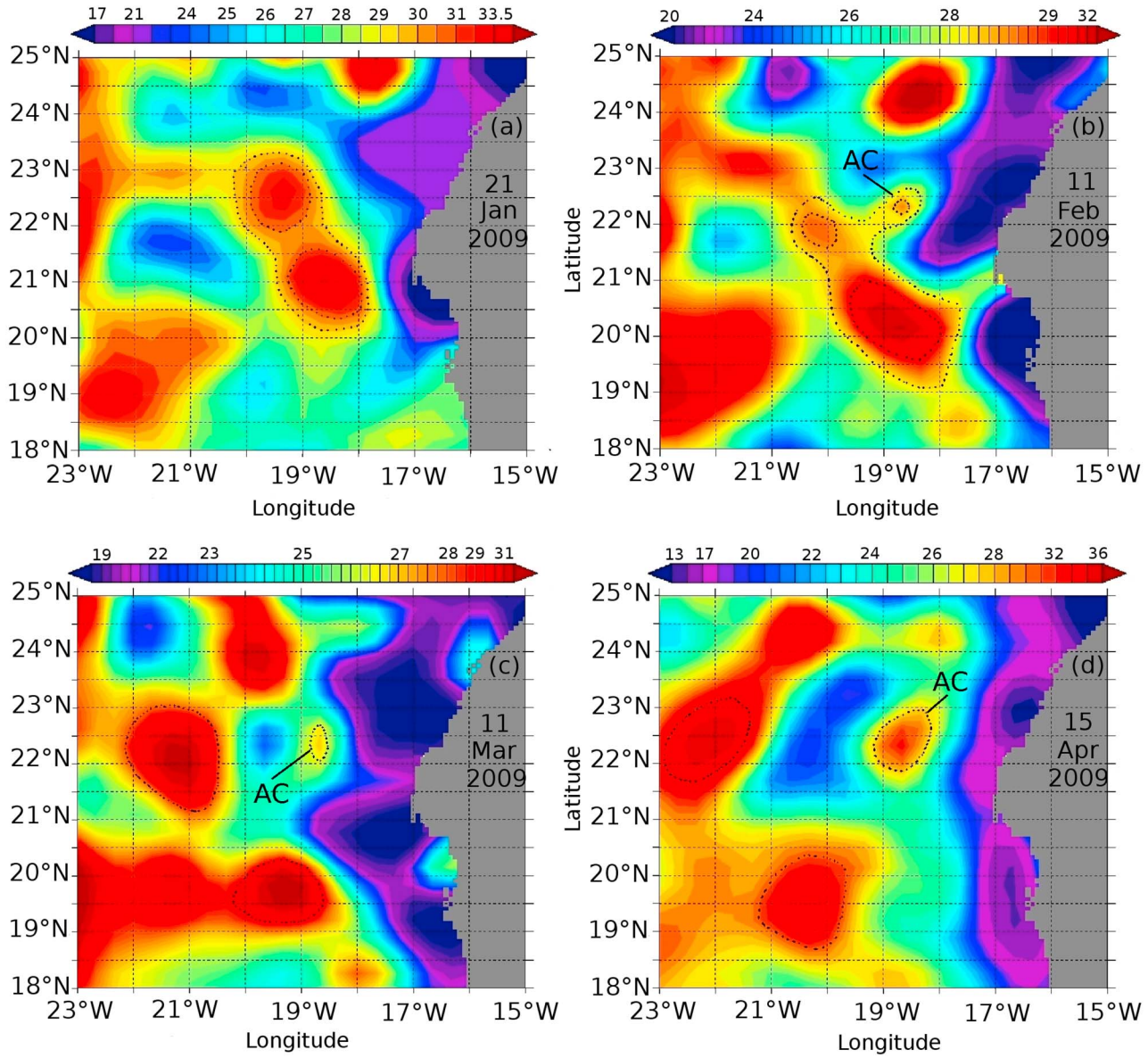

Figure 6. Absolute dynamic topography of the sea surface on (a) 21 January, (b) 11 February, (c) 11 March, and (d) 15 April 2009. The dotted contours highlight features discussed in the text. The anticyclone is marked 'AC'.

the dynamic topography and the geostrophic velocity field, as well as in the SST maps in Figure 3.

[33] The velocity fields at 24 and 288 m superimposed on the surface spiciness are shown in Figure 9. The current pattern can be split into 4 regions with distinct behavior. These regions are represented by the purple ellipses. The filament is obvious in the spiciness map as a hammer head of low spiciness water extending from 18.2 to 19°W and centered at about 20.6°N. It is bounded at the south, west and north (respectively regions B, C and D) by higher spiciness water pools and at the east by a wide meridional strip of low spiciness water (region A). The velocity associated with the filament is essentially directed offshore west of 18.2°W over the upper 288 m. North of the filament (region D), there is a clear anticyclonic circulation associated with the circular patch of high spiciness, resulting in intense offshore current. West of the filament (region C), a southward current is obvious over the entire water column. This reversal of the velocity coincides well with the temperature and spiciness front which bounds the filament to the west. The velocity field south of the filament (region B) is harder to characterize, as zones of convergence and divergence are superimposed on a general cyclonic recirculation. These complicated patterns may be attributed to the rapid evolution of the filament and the lack of synopticity of the survey, but could also be associated with submesoscale activity also observable in the SST maps in Figure 3. Internal and inertial waves may also affect the observed velocity field. Finally, east of 18°W, a northward flow, contouring anticyclonically the base of the Cap Blanc filament is obvious over the low-spiciness strip. The north-westward flow associated with the low spiciness strip entering the surveyed area from the south and

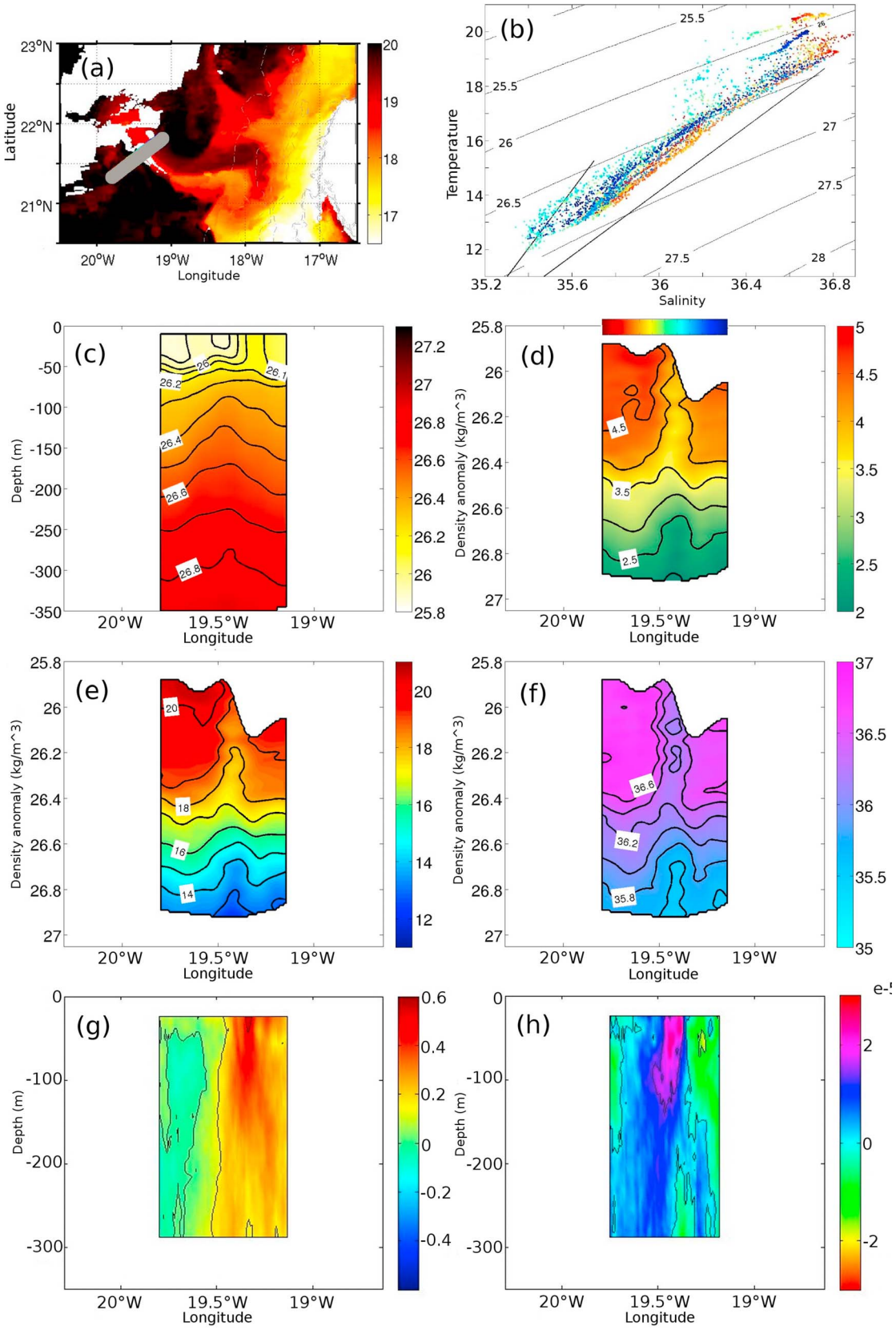

Figure 7. (a) Section L1T3 location superimposed on SST map of 17 April. (b) TS diagram for transect in which data point locations are indicated by the reference colors superimposed on the section trajectory above Figure 7d. Vertical sections of (c) in situ density against depth and (d) spiciness, (e) temperature and (f) salinity against density across the eddy. (g) Current speed and (h) relative vorticity against depth.

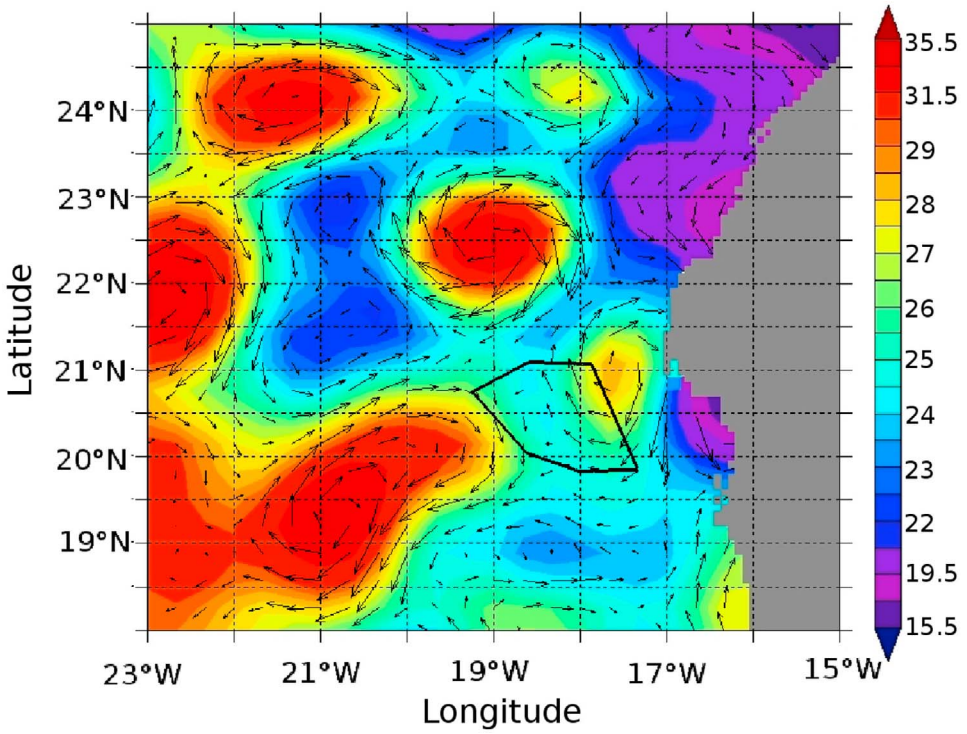

Figure 8. Absolute geostrophic velocity field (arrows) superposed on absolute dynamic topography (color) on 06 May 2009. The surveyed area is indicated on the right hand side of the map by a black polygon.

contouring the base of the promontory is thus related with this anticyclone. Unfortunately, the coarse resolution of the altimetric data (25 km) does not allow a precise characterization of the geostrophic velocity field and topographic signature of the filament itself.

[34] The distributions of spiciness on the 26.2, 26.4 and 26.8 isopycnal surfaces are shown in Figure 10. Upwelling is evident as the outcropping of the 26.2 isopycnal near the shelf break and a rise of the 26.4 isopycnal from about 120 m over the slope to 20 m on the shelf. The filament structure, evident in the form of ridging of the 26.2 and 26.4 isopycnals, has a north-east/south-west orientation just north of the cap Blanc promontory in good agreement with the SST signature visible in Figure 3. No sign of the filament is visible on the 26.8 surface, whose main feature is a strong north-east/south-west orientated ridge-like depth anomaly centered at 20.5°N 18.5°W.

[35] The filament is well defined on the 26.2 isopycnal surface as a zonal tongue of low (<3.8) spiciness. As mentioned above, several masses of high spiciness water

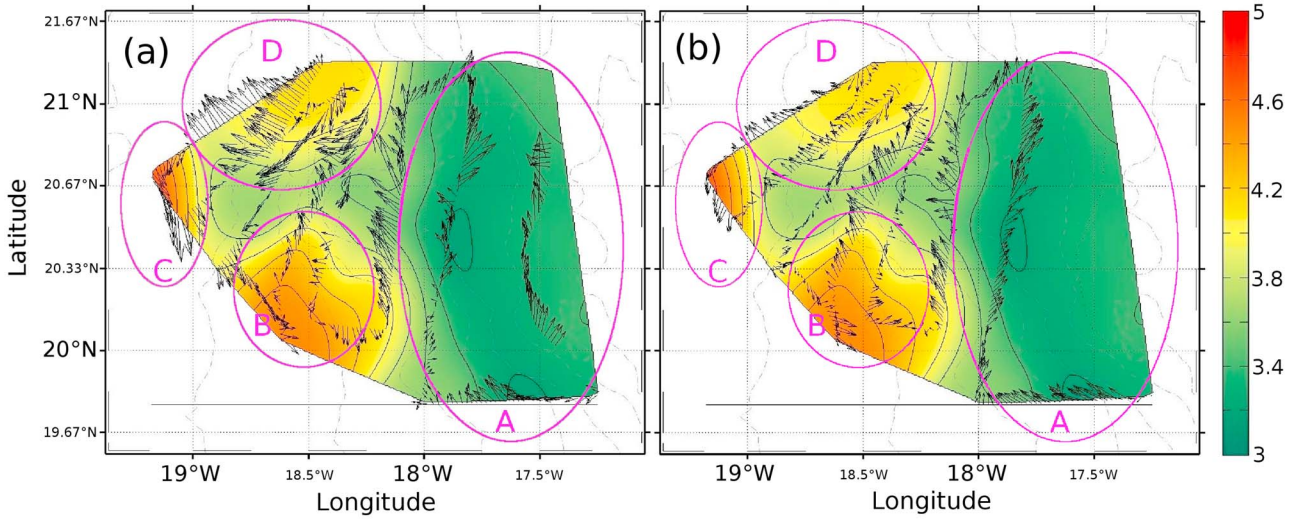

Figure 9. Velocity field at (a) 24 and (b) 288 m during the second survey superimposed on spiciness map at 5 m depth. The ellipses define regions discussed in the text.

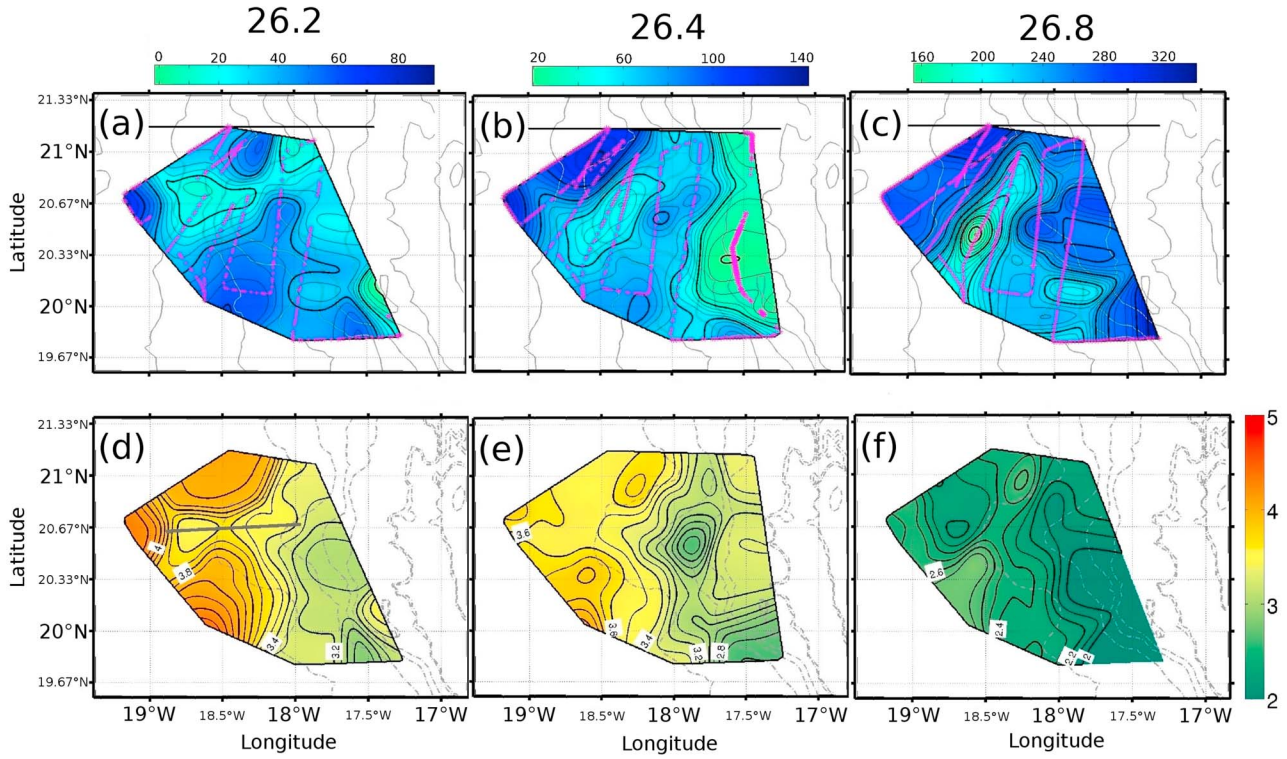

Figure 10. Second survey, depth of the (a) 26.2, (b) 26.4 and (c) 26.8 isopycnal surfaces. (d–f) Spiciness on these surfaces.

(up to 4.2) surround the filament, whose tip splits to roll cyclonically around the spicy southern body water and anticyclonically around the northern one. On the 26.4 isopycnal, the filament spiciness gradients are weaker, so that only a gentle meander is observed offshore of 18°W. The strip of low spiciness extending north all across the surveyed area becomes more obvious on the 26.4 isopycnal, reaching a minimum value (<2.8) as a circular patch centered at 20.5°N 17.8°W . This band of cooler and fresher water is advected from the south by the northward current flowing around the promontory (Figures 9 and 12h), which is associated with the recently formed anticyclonic eddy centered over the Cap Blanc promontory (Figure 8). On the 26.8 isopycnal surfaces, the filament signal is only evident as a meander of the low spiciness strip.

[36] The L2T6 section (Figure 11) crossed the central part of the filament, between 21°N 18.3°W and 20.2°N 18.5°W. The 26 to 26.2 isopycnals outcropped south of the filament. The sharp doming of the 26.3 isopycnal is a good indicator of the filament's center in terms of density anomaly. At depths below the 26.5 isopycnal, the filament is hardly discernible. An intrusion of low spiciness water is evident between 20.5 and 20.8°N between the 26.4 isopycnal and the surface. The corresponding signal in terms of temperature, salinity and spiciness has the form of a steep dome, with isolines crossing the isopycnals in the first 100 m. This structure is bounded on both side by high salinity/spiciness water. The filament is hardly visible below the 26.6 isopycnal.

[37] In the section across the slope at 19.7°N, isopycnals above 150 m rise toward the shelf, consistent with shelf-break upwelling, and the 26.2 to 25.9 isopycnals outcrop (Figure 12). Below 150 m, all isopycnals bend strongly downward toward the continental slope, e.g. the 26.8 isopycnal sinks from 200 m at 18°W to 350 m at 17.3°W. The salinity and temperature structure in isopycnic coordinates clearly shows a water mass front between 18 and 17.7°W indicated by a rise of the 35.6 isohaline from the 26.7 to 26.3 isopycnals. The Cape Verde frontal zone, which separates SACW to NACW, was defined by *Perez-Rodriguez et al.* [2001] as a strong salinity gradient along the 26.5 or larger isopycnals, seen here, corresponding roughly to the 16°C isotherm.

[38] This sharp front thus separates fresh (<35.5 psu) and cool SACW over the slope from warmer and saltier water offshore, consistent with NACW. Just below the surface, between the 26.3 and 26.2 isopycnal, a small patch of warmer, saltier water lies east of the low salinity water, separating the SACW strip from the coast. A section of meridional velocity (Figure 12) shows that the northward flow is intensified offshore of the shelf break near the surface. It reaches 0.4 m.s^{-1} above 50 m near 17.7°W. The flow is horizontally sheared near the shelf-break (10^{-6} s^{-1}), and is near-zero at 17.3°W. This northward flow, related with the anticyclonic eddy over the promontory (Figure 8) advects SACW along the slope, then into the filament.

4. Discussion and Conclusion

[39] The results presented here strongly suggest that the Cap Blanc filaments result from the contribution of several processes associated with eddy dynamics. Remotely sensed, ADCP and hydrographic data all clearly showed the close relationship between the anticyclonic eddy (AC) surveyed during the first leg of the experiment and the long filament

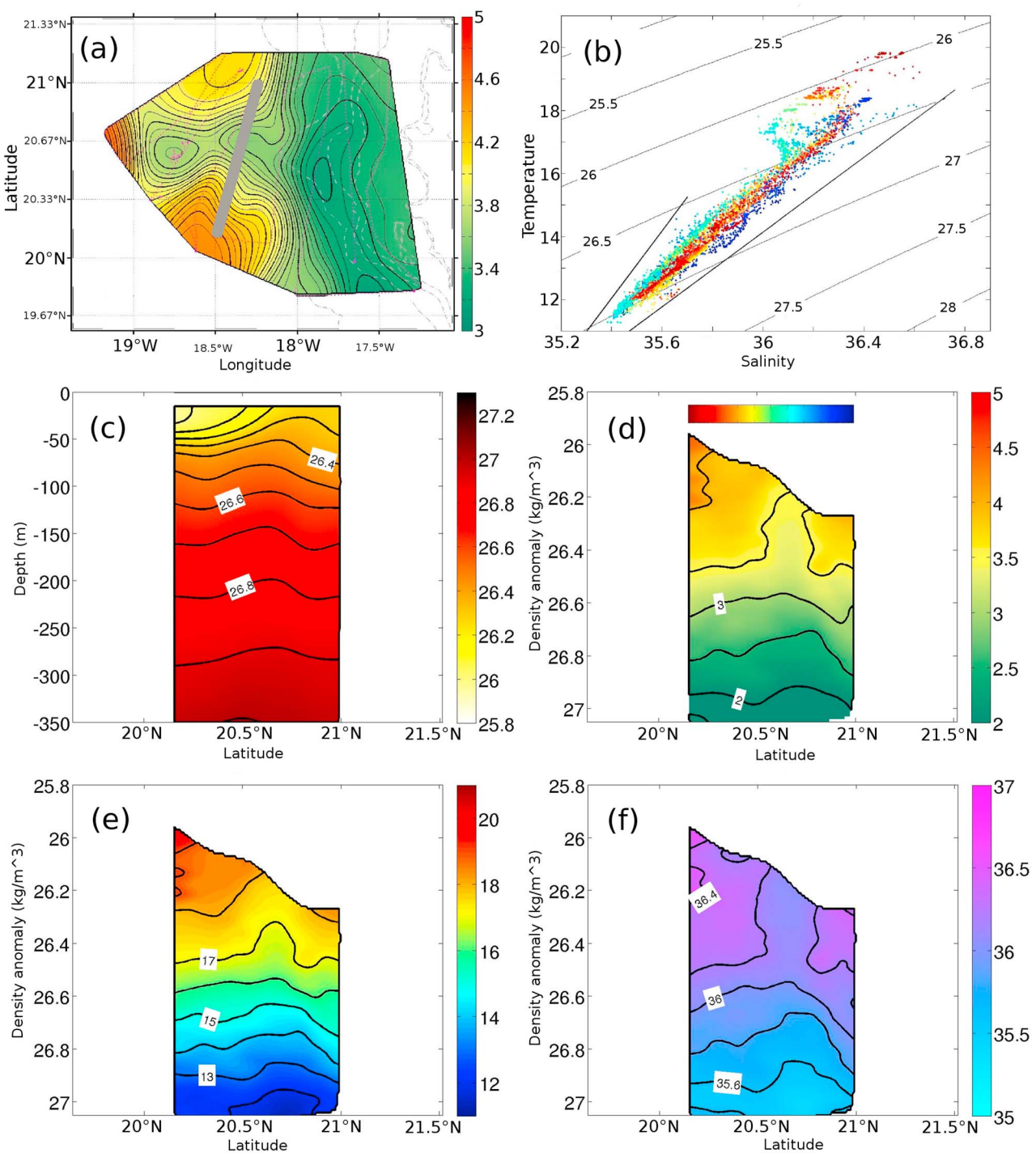

Figure 11. (a) Section L2T6 location superimposed on a sea surface spiciness map. (b) TS diagram for transect in which of data point locations are indicated by the reference colors superimposed on the spiciness section. Vertical sections of (c) in situ density against depth and (d) spiciness, (e) temperature, and (f) salinity against density across the eddy section.

entrained around the latter. They also suggested that a near-coastal anticyclone surveyed during the second leg, probably related with topographic effects played a prime role in advecting northwestward SACW water into the base of the upwelling filament. The impact of eddies on the formation and growth of filaments from coastal fronts was also observed in satellite imagery by *Shapiro et al.* [2010] in the Black sea and by *Serra et al.* [2010] in the southern Iberian upwelling system. Moreover, most processes recognized to trigger the filamentation of a front are associated with vortical structures, whether they originate from topographic effects [*Meunier et al.*, 2010; *Barton et al.*, 2004], instability processes [*Ikeda and Emery*, 1984; *Marchesiello et al.*,

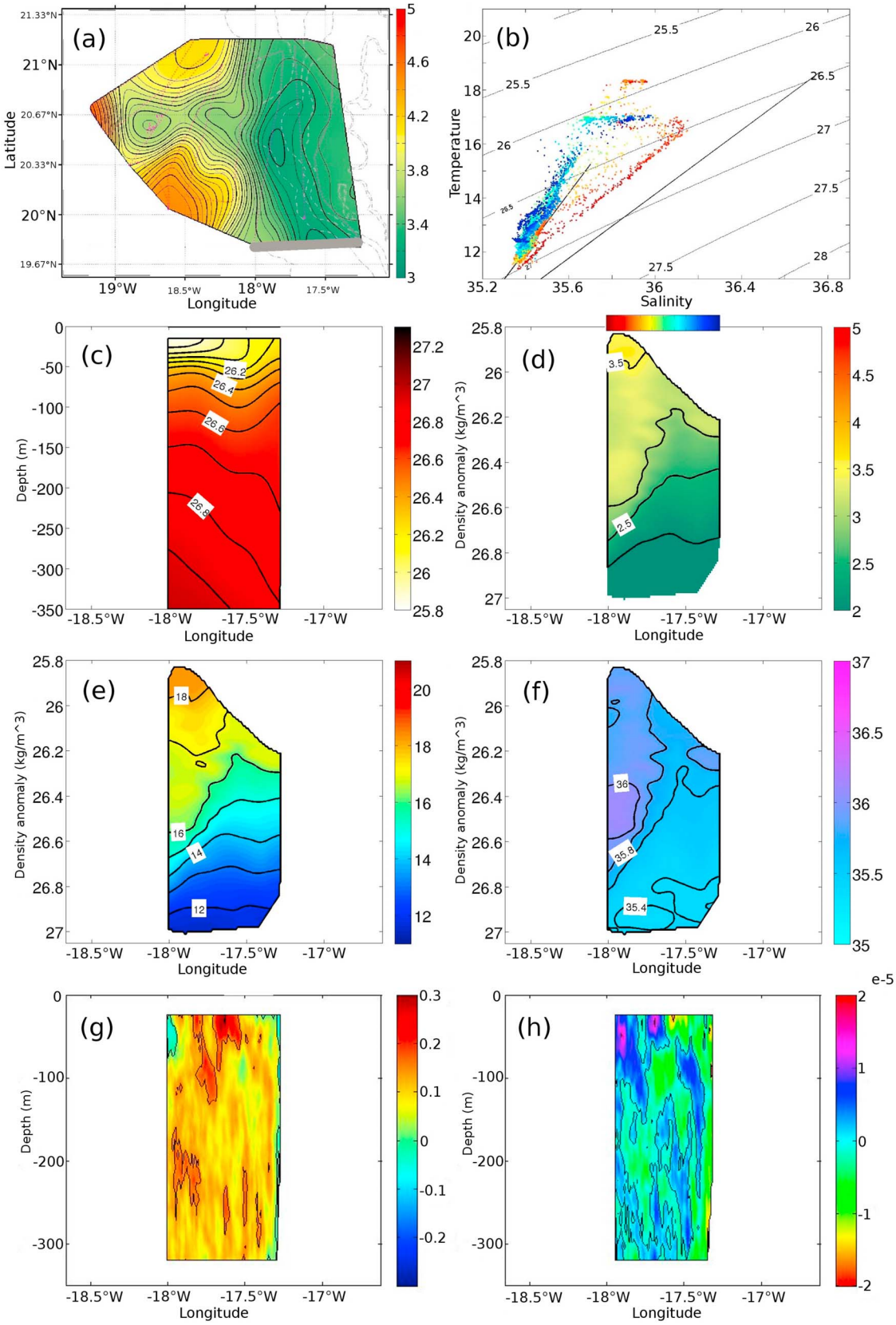

Figure 12. (a) Section L2T9 location superimposed on a sea surface spiciness map. (b) TS diagram for transect in which of data point locations are indicated by the reference colors superimposed on the spiciness section. Vertical sections of (c) in situ density against depth and (d) spiciness, (e) temperature, and (f) salinity against density across the eddy section. (g) Current speed and (h) relative vorticity against depth.

2003; *Capet and Carton*, 2004; *Meunier et al.*, 2012] or external sources [*Strub et al.*, 1991].

[40] However, this is the first time to our knowledge that an upwelling filament and its tangent eddy are sampled together in-situ with resolution sufficient to evaluate and compare the velocity and vorticity of the filament and eddy. The great similarity between the dynamical structure of the filament and neighboring anticyclone strongly suggests that here, the eddy is mostly driving the circulation along the filament. This apparent domination of the eddy velocity field over the filament's intrinsic geostrophic circulation might not be as obvious in other upwelling systems where a stronger stratification would enhance the intrinsic flow associated with the density anomaly within the filament.

[41] The size of the observed anticyclone (AC) matches well the typical spatial scale of the instability-induced eddies of the CVFZ (0(100 km)) [*Onken and Klein*, 1991]. The altimetric data from the eddy's formation and its thermohaline structure also suggest that the origin of the eddy can be related to the Cape Verde front: the anticyclone AC was shown to arise from the interaction of two previously formed anticyclones in the vicinity of the frontal zone which was recognized to be a great mesoscale eddy source [*Onken and Klein*, 1991], and the core of the eddy was shown to contain both water masses: SACW at depth and NACW near the surface. In the absence of diabatic processes, temperature and salinity are conserved within the eddy core. The water masses trapped within the eddy thus remain unchanged since the eddy's formation, meaning that the water column captured in the eddy was formed in the vicinity of both NACW and SACW, namely in the Cape Verde frontal zone. Of course, diabatic processes such as horizontal and vertical mixing, or radiative and latent heat fluxes at the sea surface do happen in this region, but tracer conservation is still strong enough for the water masses to remain identifiable. The Cape Verde front eddy field then seems to be a key element in the generation of the Cap Blanc filaments. This results are consistent with *Strub et al.*'s [1991] idea that filament formation can arise from the interaction of an upwelling front and an external mesoscale eddy field. As eddies drift westward, and upwelling current systems mainly occur along eastern boundaries, the possibility for an external eddy field to interact with the upwelling is unlikely and most eddies interacting with upwelling fronts are likely to be intrinsically generated by the current. From that point of view, Cap Blanc might be one of the few places in the world ocean where this process could be observed.

[42] The second leg of the survey showed a different case of the role of eddies in the dynamics of the Cap Blanc filaments. A large anticyclone centered over the Cap Blanc promontory was identified in the altimetric data and in the ADCP data. It was found to be responsible for the northwestward advection of SACW water in the form of a strip of low spiciness water, which subsequently was exported offshore within the filament. The position of the anticyclone, just above the promontory suggests that it may have formed from topographic processes. *Barton et al.* [2004] reported the presence of a recurrent cyclone in the Cabo Juby region (Morocco) which was related with a topographic trough. The dynamics of the topographic generation and trapping of eddies and their impact on upwelling filaments formation was studied by *Meunier et al.* [2010]. They showed that the spin up of an along shore barotropic current induced by the set up of an along shore wind produced trapped anticyclones over promontories and cyclones over troughs, and that these trapped eddies could trigger the formation of long lived filaments. Indeed, as the currents set up, they advect low PV parcels from deep areas into the promontory and high PV parcels from the promontory into deeper areas, resulting in the generation of PV anomalies in the form of a trapped anticyclone and a freely evolving cyclone. The location of the anticyclone over the promontory, as well as the fact that it formed in a few days just after a reintensification of the wind suggests that it is associated with such topographic processes.

[43] One of the main peculiarities of the Cap Blanc filaments is the contrast between the thermohaline properties of the water they transport and those of the surrounding water: the hydrographic maps on isopycnal surfaces exhibited considerable variability of temperature and salinity. In all vertical sections in density coordinates, isotherms, and more obviously isohalines were seen to cross the isopycnal levels. In the absence of diabatic processes, both temperature and salinity are conserved along an isopycnal path. therefore, the crossing of isopycnal lines by isohalines and isotherms is evidence of horizontal transport of different water masses. If diabatic processes were responsible for the observed cross-isopycnal excursions, they would appear more randomly in the entire surveyed area and not particularly within the filaments. The presence of the topographic anticyclone plays a significant role in the feeding of filament C with this distinct water.

[44] Finally, the rapid evolution of the Cap Blanc filaments is striking. SST images showed that it only took about 10 days for filament C to grow from a small amplitude meander into a long filament and to be transformed into a low coherence multi-filament decaying structure. Whereas in the northern part of the NW African upwelling system, filaments can be observed for over a month [*Barton*, 1998], the filaments observed during the ICON cruise have short life cycles. The formation of shorter filaments south of the Banc d'Arguin, and their rapid northward propagation seemed to play a role in the rapid alteration of filament C. It is unclear whereas these structures are associated with baroclinic instability of the upwelling front or with the interaction of the latter with mesoscale to submesoscale features. The observation of submesoscale to small scale structures in the form of 'bubbles' and lenses of contrasting temperature and salinity associated with zones of apparent ageostrophic currents, with convergences and divergences suggest that the Cap Blanc region is rich in highly spatially variable processes, which could explain the rapid alteration of the mesoscale structures.

[45] The dynamics and hydrography of the Cap Blanc filaments appear to result from a complex chain of processes associated with a peculiar hydrography. Naturally, SACW and NACW are likely to be found respectively south and north of the domain, but the frontier between the two water masses was shown not to be strictly zonal, as SACW tends to be advected northward over the continental shelf and slope north of the Banc d'Arguin [*Mittelstaedt*, 1991]. Here, it was shown that the SACW, initially carried by a poleward current south of the surveyed region [*Barton et al.*, 1977] was then transported anticyclonically around the Cap Blanc promontory by a coherent eddy which is consistent with a topographically controlled anticyclone. Once the water mass

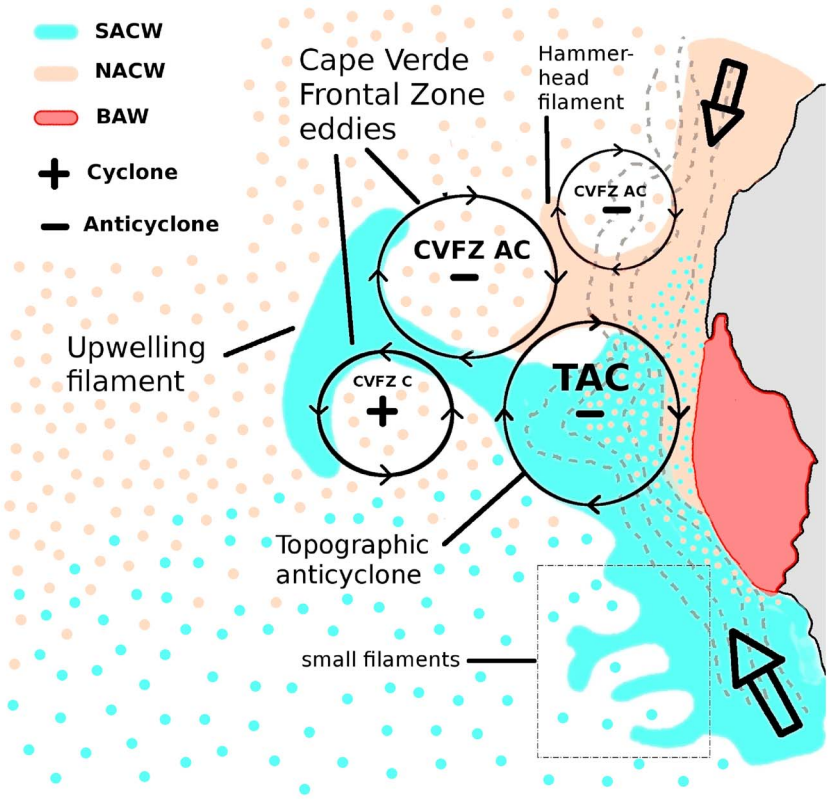

Figure 13. Schematic Cap Blanc filament dynamics: SACW (blue) entering the region from the south via the poleward current is relayed around the topographic anticyclone (TAC), and extended further from the coast around offshore eddies associated with the CVFZ (C and AC), similar to filament A and the 'AC' anticyclone sampled during leg 1. Further north, the upwelling jet carries NACW (light orange) equatorward. The offshore eddy field also triggers filament formation like the observed hammer-head structure during leg 1 (filament B). The red area represents the isolated warm Banc d'Arguin Water (BAW). Solid and dotted colors represent upwelled and non-upwelled water, respectively.

has reached the tip of the promontory, offshore eddies associated with the CVFZ relieve the topographic eddy and entrain the water far offshore. Note that while the topographic process tends to form recurrent and trapped filaments, the external eddies detrain the fluid randomly along the coastline. This perhaps unique chain of eddies of different nature entrains the coastal SACW offshore like a gearing, as shown in the schematic view of Figure 13.

[46] **Acknowledgments.** The field work and analysis was supported principally by UK NERC grant NE/C517176/2. Analysis was also supported by grant CTM2008-05305-E/MAR of the Spanish Ministerio de Educacion y Ciencia. The authors thank the NERC Earth Observation Data Acquisition and Analysis Service (NEODAAS) and IFREMER-CERSAT for supplying data for this study. They are also grateful to the National Marine Facility staff from the Discovery cruise D338 for their great professionalism in managing the MVP data. T.M. is indebted to Xavier Carton and Steven Herbette whose suggestions helped to improve the manuscript. This study is part of T.M.'s PhD thesis supported by a grant from the French Ministry of Research.

References

Alvarez-Salgado, X. A., M. D. Doval, A. V. Borges, M. Joint, I. Frankignoulle, M. Woodward, and F. G. Figueiras (2001), Off-shelf fluxes of labile materials by an upwelling filament in the NW Iberian Upwelling System, *Prog. Oceanogr.*, *51*, 321–337, doi:10.1016/S0079-6611(01)00073-8.

Barnes, S. L. (1994), Applications of the Barnes objective analysis scheme. Part I: Effects of undersampling, wave position, and station randomness, *J. Atmos. Oceanic Technol.*, *11*, 1433–1448, doi:10.1175/1520-0426(1994)0112.0.CO;2.

Barton, E. D. (1987), Meanders, eddies and intrusions in the Central Water Mass Front off NW Africa, *Oceanol. Acta*, *10*, 267–283.

Barton, E. (1998), The transition zone of the Canary Current upwelling region, *Prog. Oceanogr.*, *41*, 455–504, doi:10.1016/S0079-6611(98)00023-8.

Barton, E., A. Huyer, and E. L. Smith (1977), Temporal variation observed in the hydrographic regime near Cabo Corveiro in the northwest African upwelling region, February to April 1974, *Deep Sea Res., Part II*, *24*, 7–23, doi:10.1016/0146-6291(77)90537-9.

Barton, E., P. Hughes, and J. H. Simpson (1982), Vertical shear observed at contrasting sites over the continental slope off NW Africa, *Oceanol. Acta*, *5*, 169–178.

Barton, E. D., M. E. Inall, T. J. Sherwin, and R. Torres (2001), Vertical structure, turbulent mixing and fluxes during Lagrangian observations of an upwelling filament system off northwest Iberia, *Prog. Oceanogr.*, *51*, 249–267, doi:10.1016/S0079-6611(01)00069-6.

Barton, E. D., J. Aristegui, T. Tett, and E. Navarro-Pérrez (2004), Variability in the Canary Islands area of filament-eddy exchanges, *Prog. Oceanogr.*, *62*, 71–94, doi:10.1016/j.pocean.2004.07.003.

Batteen, M. L. (1997), Wind-forced modeling studies of currents, meanders, and eddies in the California Current system, *J. Geophys. Res.*, *102*(C1), 985–1010, doi:10.1029/96JC02803.

Batteen, M. L., A. S. Martinho, H. A. Miller, and J. L. McClean (2007), A process-oriented study of the Coastal Canary and Iberian Current System, *Ocean Modell.*, *18*, 1–36, doi:10.1016/j.ocemod.2007.02.006.

Brink, K. (1983), The near-surface dynamics of coastal upwelling, *Prog. Oceanogr.*, *12*, 223–257, doi:10.1016/0079-6611(83)90009-5.

Capet, X. J., and X. J. Carton (2004), Nonlinear regimes of baroclinic boundary currents, *J. Phys. Oceanogr.*, *34*(6), 1400–1409, doi:10.1175/1520-0485(2004)0342.0.CO;2.

Capet, X. J., L. Chérubin, and Y. Morel (2002), Influence of the transport on the instability of a boundary current, *J. Phys. Oceanogr.*, *32*(10), 2806–2815, doi:10.1175/1520-0485(2002)0322.0.CO;2.

Capet, X., J. C. McWilliams, M. J. Molemaker, and A. F. Shchepetkin (2008a), Mesoscale to submesoscale transition in the California Current System. Part I: Flow structure, eddy flux, and observational tests, *J. Phys. Oceanogr.*, *38*, 29–43, doi:10.1175/2007JPO3671.1.

Capet, X., J. C. McWilliams, M. J. Molemaker, and A. F. Shchepetkin (2008b), Mesoscale to submesoscale transition in the California Current System. Part II: Frontal processes, *J. Phys. Oceanogr.*, *38*, 44–64, doi:10.1175/2007JPO3672.1.

Capet, X., J. C. McWilliams, M. J. Molemaker, and A. F. Shchepetkin (2008c), Mesoscale to submesoscale transition in the California Current System. Part III: Energy balance and flux, *J. Phys. Oceanogr.*, *38*, 2256–2269, doi:10.1175/2008JPO3810.1.

Carton, X. J., and B. Legras (1994), The life-cycle of tripoles in two-dimensional incompressible flows, *J. Fluid Mech.*, *267*, 53–82, doi:10.1017/S0022112094001114.

Dewey, R. K., J. N. Moum, C. A. Paulson, D. R. Caldwell, and S. D. Pierce (1991), Structure and dynamics of a coastal filament, *J. Geophys. Res.*, *96*, 14,885–14,907, doi:10.1029/91JC00944.

Emery, J., and J. Meincke (1986), Global water masses: Summary and review, *Oceanol. Acta*, *9*, 383–391.

Erasmi, W., G. Siedler, and R. Onken (1998), Energy conversion in the Cape Verde Frontal Zone, *J. Geophys. Res.*, *103*, 21,469–21,480, doi:10.1029/98JC01887.

Firing, E., J. Ranada, and P. Caldwell (1995), Processing ADCP data with the CODAS software system version 3.1, user's manual, technical report, 212 pp., Jt. Inst. for Mar. and Atmos. Res., Univ. of Hawai'i at Mānoa, Honolulu.

Flament, P. (2002), A state variable for characterizing water masses and their diffusive stability: Spiciness, *Prog. Oceanogr.*, *54*, 493–501, doi:10.1016/S0079-6611(02)00065-4.

Flament, P., L. Armi, and L. Washburn (1985), The evolving structure of an upwelling filament, *J. Geophys. Res.*, *90*, 11,765–11,778, doi:10.1029/JC090iC06p11765.

Fofonoff, N. P., and R. C. Millard (1983), Algorithms for computation of fundamental properties of seawater, *Tech. Pap. Mar. Sci.*, 44, 53 pp., U.N. Educ., Sci. and Cult. Organ., Paris.

Fraga, F. (1974), Distribution des masses d'eau dans l'upwelling de Mauritanie, *Thetys*, *6*, 5–10.

Gabric, A. J., L. Garcia, L. Van Camp, L. Nykjaer, W. Eifler, and W. Schrimpf (1993), Offshore export of shelf production in the Cape Blanc (Mauritania) giant filament as derived from coastal zone color scanner imagery, *J. Geophys. Res.*, *98*, 4697–4712, doi:10.1029/92JC01714.

Haidvogel, D. B., A. Beckmann, and K. S. Hedström (1991), Dynamical simulations of filament formation and evolution in the coastal transition zone, *J. Geophys. Res.*, *96*, 15,017–15,040, doi:10.1029/91JC00943.

Haynes, R., E. D. Barton, and I. Pilling (1993), Development, persistence and variability of upwelling filaments off the Atlantic coast of the Iberian Peninsula, *J. Geophys. Res.*, *98*, 22,681–22,692, doi:10.1029/93JC02016.

Hughes, P., and E. D. Barton (1974), Stratification and water mass structure in the upwelling area off northwest Africa in April/May 1969, *Deep Sea Res. Oceanogr. Abstr.*, *21*(8), 611–628, doi:10.1016/0011-7471(74)90046-1.

Ikeda, M., and J. R. Apel (1981), Mesoscale eddies detached from spatially growing meanders in an eastward-flowing oceanic jet using a two-layer quasi-geostrophic model, *J. Phys. Oceanogr.*, *11*, 1638–1661, doi:10.1175/1520-0485(1981)0112.0.CO;2.

Ikeda, M., and W. J. Emery (1984), Satellite observations and modeling of meanders in the California Current System off Oregon and northern California, *J. Phys. Oceanogr.*, *14*, 1434–1450, doi:10.1175/1520-0485(1984)0142.0.CO;2.

Ikeda, M., J. A. Johannessen, K. Lygre, and S. Sandven (1989), A process study of mesoscale meanders and eddies in the Norwegian Coastal Current, *J. Phys. Oceanogr.*, *19*, 20–35, doi:10.1175/1520-0485(1989)0192.0.CO;2.

Klein, B., and G. Siedler (1995), Isopycnal and diapycnal mixing at the Cape Verde Frontal Zone, *J. Phys. Oceanogr.*, *25*, 1771–1787, doi:10.1175/1520-0485(1992)0222.0.CO;2.

Knoll, M., A. Hernández-Guerra, B. Lenz, F. López Laatzen, F. Machín, T. J. Müller, and G. Siedler (2002), The Eastern Boundary Current system between the Canary Islands and the African Coast, *Deep Sea Res., Part II*, *49*, 3427–3440, doi:10.1016/S0967-0645(02)00105-4.

Kostianoy, A. G., and A. G. Zatsepin (1996), The West African coastal upwelling filaments and cross-frontal water exchange conditioned by them, *J. Mar. Syst.*, *7*, 349–359, doi:10.1016/0924-7963(95)00029-1.

Lutjeharms, J. R. E., F. A. Shillington, and C. M. Duncombe Rae (1991), Observations of extreme upwelling filaments in the southeast Atlantic Ocean, *Science*, *253*, 774–776, doi:10.1126/science.253.5021.774.

Marchesiello, P., and P. Estrade (2009), Eddy activity and mixing in upwelling systems: A comparative study of Northwest Africa and California regions, *Int. J. Earth Sci.*, *98*, 299–308, doi:10.1007/s00531-007-0235-6.

Marchesiello, P., J. C. McWilliams, and A. Shchepetkin (2003), Equilibrium structure and dynamics of the California Current System, *J. Phys. Oceanogr.*, *33*, 753–783, doi:10.1175/1520-0485(2003)332.0.CO;2.

Marin, V. H., R. Escribano, L. E. Delgado, G. Olivares, and P. Hidalgo (2001), Nearshore circulation in a coastal upwelling site off the Northern Humboldt current system, *Cont. Shelf Res.*, *21*, 1317–1329, doi:10.1016/S0278-4343(01)00022-X.

Martínez-Marrero, A., A. Rodríguez-Santana, A. Hernández-Guerra, E. Fraile-Nuez, F. López-Laatzen, P. Vélez-Belchí, and G. Parrilla (2008), Distribution of water masses and diapycnal mixing in the Cape Verde Frontal Zone, *Geophys. Res. Lett.*, *35*, L07609, doi:10.1029/2008GL033229.

Meunier, T., V. Rossi, Y. Morel, and X. Carton (2010), Influence of bottom topography on an upwelling current: Generation of long trapped filaments, *Ocean Modell.*, *35*(4), 277–303, doi:10.1016/j.ocemod.2010.08.004.

Meunier, T., X. Carton, and R. Duarte (2012), Influence of a deep flow on a surface boundary current, *Geophys. Astrophys. Fluid Dyn.*, *0*(0), 1–27, doi:10.1080/03091929.2012.657190.

Mittelstaedt, E. (1991), The ocean boundary along the northwest African coast: Circulation and oceanographic properties at the sea surface, *Prog. Oceanogr.*, *26*, 307–355, doi:10.1016/0079-6611(91)90011-A.

Navarro-Perez, E., and E. D. Barton (1998), The physical structure of an upwelling filament off the north-west African coast during August 1993, *South Afr. J. Mar. Sci.*, *19*, 61–73, doi:10.2989/025776198784126827.

Onken, R., and B. Klein (1991), A model of baroclinic instability and waves between the ventilated gyre and the shadow zone of the North Atlantic Ocean, *J. Phys. Oceanogr.*, *21*, 53–67, doi:10.1175/1520-0485(1991)0212.0.CO;2.

Peliz, A., T. L. Rosa, M. P. Santos, and J. L. Pissarra (2002), Fronts, jets, and counter-flows in the Western Iberian upwelling system, *J. Mar. Syst.*, *35*, 61–77, doi:10.1016/S0924-7963(02)00076-3.

Peliz, Á., A. M. P. Santos, P. B. Oliveira, and J. Dubert (2004), Extreme cross-shelf transport induced by eddy interactions southwest of Iberia in winter 2001, *Geophys. Res. Lett.*, *31*, L08301, doi:10.1029/2004GL019618.

Perez-Rodriguez, P., J. L. Pelegri, and A. Marrero-Diaz (2001), Dynamical characteristics of the Cape Verde frontal zone, *Sci. Mar.*, *65*, 241–250.

Ramp, S. R., P. F. Jessen, K. H. Brink, P. P. Niiler, F. L. Daggett, and J. S. Best (1991), The physical structure of cold filaments near Point Arena, California, during June 1987, *J. Geophys. Res.*, *96*, 14,859–14,883, doi:10.1029/91JC01141.

Relvas, P., and E. D. Barton (2002), Mesoscale patterns in the Cape São Vicente (Iberian Peninsula) upwelling region, *J. Geophys. Res.*, *107*(C10), 3164, doi:10.1029/2000JC000456.

Røed, L. P., and X. B. Shi (1999), A numerical study of the dynamics and energetics of cool filaments, jets, and eddies off the Iberian Peninsula, *J. Geophys. Res.*, *104*, 29,817–29,842, doi:10.1029/1999JC900175.

Serra, N., I. Ambar, and D. Boutov (2010), Surface expression of Mediterranean Water dipoles and their contribution to the shelf/slope–open ocean exchange, *Ocean Sci.*, *6*, 191–209, doi:10.5194/os-6-191-2010.

Shapiro, G. I., S. V. Stanichny, and R. R. Stanychna (2010), Anatomy of shelf–deep sea exchanges by a mesoscale eddy in the North West Black Sea as derived from remotely sensed data, *Remote Sens. Environ.*, *114*(4), 867–875, doi:10.1016/j.rse.2009.11.020.

Shillington, F. (1990), A cool upwelling filament off Namibia, southwest Africa: Preliminary measurements of physical and biological features, *Deep Sea Res., Part I*, *37*, 1753–1772, doi:10.1016/0198-0149(90)90075-7.

Sobarzo, M., and D. Figueroa (2001), The physical structure of a cold filament in a Chilean upwelling zone (Peninsula de Mejillones, Chile, 23°S), *Deep Sea Res., Part I*, *48*, 2699–2726, doi:10.1016/S0967-0637(01)00031-0.

Spall, M. A. (1992), Rossby wave radiation in the Cape Verde Frontal Zone, *J. Phys. Oceanogr.*, *22*, 796–807, doi:10.1175/1520-0485(1992)0222.0.CO;2.

Stern, M. E. (1986), On the amplification of convergences in coastal currents and the formation of "squirts," *J. Mar. Res.*, *44*, 403–421, doi:10.1357/002224086788403097.

Strub, P. T., P. M. Kosro, and A. Huyer (1991), The nature of the cold filaments in the California Current System, *J. Geophys. Res.*, *96*, 14,743–14,768, doi:10.1029/91JC01024.

Sverdrup, H. U., M. W. Johnson, and R. H. Flemming (1942), *The Oceans, Their Physics, Chemistry, and General Biology*, Prentice-Hall, New York.

Tomczak, M. (1981), An analysis of mixing in the frontal zone of South and North Atlantic Central Water off north-west Africa, *Prog. Oceanogr.*, *10*, 173–192, doi:10.1016/0079-6611(81)90011-2.

Traganza, E. D., D. A. Nestor, and A. K. McDonald (1980), Satellite observations of a nutrient upwelling off the coast of California, *J. Geophys. Res.*, *85*, 4101–4106, doi:10.1029/JC085iC07p04101.

Washburn, L., and L. Armi (1988), Observations of frontal instabilities on an upwelling filament, *J. Phys. Oceanogr.*, *18*, 1075–1092, doi:10.1175/1520-0485(1988)0182.0.CO;2.

Zenk, W., B. Klein, and M. Schroder (1991), Cape Verde frontal zone, *Deep Sea Res.*, *38*, 505–530.